



RESEARCH LETTER

10.1002/2017GL075721

Key Points:

- First direct measurements of the helical flow structure of turbidity currents shown as they travel around a bend
- Turbidity currents of different thicknesses and velocities exhibit the same helical flow structure
- We reconcile current controversy with a new model that explains helical flow structure for a wide range of geophysical flows

Supporting Information:

- Supporting Information S1

Correspondence to:

M. Azpiroz-Zabala,
m.azpiroz@soton.ac.uk

Citation:

Azpiroz-Zabala, M., Cartigny, M. J. B., Sumner, E. J., Clare, M. A., Talling, P. J., Parsons, D. R., & Cooper, C. (2017). A general model for the helical structure of geophysical flows in channel bends. *Geophysical Research Letters*, 44, 11,932–11,941. <https://doi.org/10.1002/2017GL075721>

Received 20 SEP 2017

Accepted 21 NOV 2017

Accepted article online 30 NOV 2017

Published online 11 DEC 2017

©2017. The Authors.

This is an open access article under the terms of the Creative Commons Attribution License, which permits use, distribution and reproduction in any medium, provided the original work is properly cited.

A General Model for the Helical Structure of Geophysical Flows in Channel Bends

M. Azpiroz-Zabala^{1,2} , M. J. B. Cartigny³ , E. J. Sumner¹, M. A. Clare², P. J. Talling³, D. R. Parsons⁴ , and C. Cooper⁵

¹Ocean and Earth Sciences, University of Southampton, Southampton, UK, ²National Oceanography Centre, Southampton, UK, ³Departments of Earth Sciences and Geography, University of Durham, Durham, UK, ⁴Department of Geography, Environment and Earth Sciences, University of Hull, Hull, UK, ⁵Formerly at Chevron Energy Technology Company, San Ramon, CA, USA

Abstract Meandering channels formed by geophysical flows (e.g., rivers and seafloor turbidity currents) include the most extensive sediment transport systems on Earth. Previous measurements from rivers show how helical flow at meander bends plays a key role in sediment transport and deposition. Turbidity currents differ from rivers in both density and velocity profiles. These differences, and the lack of field measurements from turbidity currents, have led to multiple models for their helical flow around bends. Here we present the first measurements of helical flow in submarine turbidity currents. These 10 flows lasted for 1–10 days, were up to ~80 m thick, and displayed a consistent helical structure. This structure comprised two vertically stacked cells, with the bottom cell rotating in the opposite direction to helical flow in rivers. Furthermore, we propose a general model that predicts the range of helical flow structures observed in rivers, estuaries, and turbidity currents based on their density stratification.

1. Introduction

Extensive submarine channels transport billions of tonnes of sediment for hundreds of kilometers, to form vast sedimentary deposits (called submarine fans) in the deep sea (Normark, 1970; Savoye et al., 2009; Shepard, 1933). The largest submarine fans are fed by highly sinuous submarine channels, suggesting that meander bends may enhance sediment transport distances (Pirmez & Imran, 2003; Straub et al., 2008). Submarine channels host powerful but episodic sediment-laden gravity currents called turbidity currents. Individual turbidity currents can transport more sediment than the annual flux from rivers worldwide (Talling et al., 2007). There are few direct observations of deep-sea turbidity currents (Cooper et al., 2016; Khrifpounoff et al., 2003; Talling et al., 2015; Vangriesheim et al., 2009). Before collection of this data set (Azpiroz-Zabala et al., 2017; Cooper et al., 2013), there were no detailed (subminute) measurements from within a meander bend in the deep sea. Instead, our understanding of meandering deep-sea channels was based on laboratory-scale experiments and numerical modeling, or on comparisons to rivers, estuaries, and saline density flows.

Rivers, estuaries, and saline underflows display a helical flow structure when passing through a bend, which can be broken into downstream and cross-stream components (Nidzieko et al., 2009; Parsons et al., 2010; Rozovskii, 1957; Sumner et al., 2014). The helical structure results from competing forces that drive the flow around a bend. Centrifugal acceleration drives fluid outward causing superelevation of the flow surface at the outer bend (Rozovskii, 1957; Thorne et al., 1985). Superelevation of the flow surface causes a pressure gradient that pushes fluid close to the bed toward the inner bend (Rozovskii, 1957; Thorne et al., 1985). Because the densest fluid in a stratified flow is near the bed, this inwardly directed pressure gradient can cause dense fluid to accumulate at the inner bend resulting in lateral stratification of the flow. Lateral stratification within the flow causes lateral pressure gradients; in particular, if dense fluid collects near the inner bend, then this will produce a near-bed pressure gradient that pushes fluid back toward the outer bend (Nidzieko et al., 2009; Sumner et al., 2014). The magnitude and rotation direction of helical flow cells is determined by the relative strengths of the above forces, which depend on the specific velocity and density structure of a flow and how this structure evolves around the bend. Helical flow is important because it strongly influences erosion and deposition within a channel and is thus a fundamental control on how channels evolve (Peakall et al., 2000; Rozovskii, 1957; Thorne et al., 1985).

Previous work has demonstrated that the helical structure can vary in two key ways. First, it can vary in the direction of rotation. Second, there can be a single helix (i.e., one rotating cell) or multiple helices stacked on top of one another (Corney et al., 2006, 2008; Imran et al., 2008). Helical circulation in rivers is dominated by a single helix that rotates in a clockwise direction when looking downstream through a left-hand bend. (Rozovskii, 1957; Thorne et al., 1985). Initial numerical models for turbidity currents suggested that helical circulation is similar to that in a river bend (Kassem & Imran, 2004). However, the first physical experiments of helical circulation in turbidity currents showed an opposite direction of rotation—with the near-bed flow moving toward the outer bank (Corney et al., 2006; Keevil et al., 2006). To complicate matters further, both directions of helical circulation (river like and river reversed) have subsequently been observed in turbidity current experiments and models, depending on flow conditions and channel morphology (Abad et al., 2011; Bolla Pittaluga & Imran, 2014; Cossu & Wells, 2010; Dorrell et al., 2013; Ezz & Imran, 2014; Giorgio Serchi et al., 2011; Huang et al., 2012; Imran et al., 2007; Islam & Imran, 2008; Janocko et al., 2013).

Flow around bends in well-mixed estuaries show a river-like basal helical circulation, while stratified estuaries and saline flows are river reversed (Nidziedo et al., 2009; Wei et al., 2013). In stratified flows, across-flow variation in stratification (i.e., flow density) sets up an additional lateral pressure gradient that is thought to play a key role in determining the direction of the flow rotation (Nidziedo et al., 2009; Sumner et al., 2014). Such stratification-triggered pressure gradients have been suggested to be important for turbidity currents, which are density stratified because of vertical variations in sediment concentration (Peakall & Sumner, 2015; Sumner et al., 2014). This hypothesis remains untested because of a lack of field-scale observations of turbidity currents.

Here we present the first direct measurements of turbidity currents at a meander bend in the ocean, including 10 flows with varying flow conditions. We use these data to determine the rotation direction of helical flow within these turbidity currents. This provides the first field test of existing numerical and experimental models. Second, we determine how flow structure varies with fluctuating flow properties and discuss the implications for the morphological evolution of submarine channel bends. Finally, we compare our results with existing field measurements in other geophysical flows and propose a general model for helical flow structure across a wide range of geophysical flows including rivers, saline density flows, and turbidity currents.

2. Study Area

Our data were recorded at 2,000 m water depth in the Congo Canyon (Azpiroz-Zabala et al., 2017; Cooper et al., 2013). The Congo Canyon is the proximal part of one of the largest submarine channel systems on Earth, which is fed directly by the Congo River (Heezen et al., 1964). The submarine channel extends for over 1,000 km, from the continental shelf to its final termination at 5,000 m water depth (Heezen et al., 1964; Khripunoff et al., 2003). The upper part of the Congo Canyon has a meandering planform with tight bends, a deeply incised thalweg, and numerous terraces (Figure 1). The Congo Canyon is a highly active system in the present day. Several turbidity currents occur each year in the upper canyon, based on cable breaks (Heezen et al., 1964) and direct flow measurements (Azpiroz-Zabala et al., 2017; Cooper et al., 2013, 2016; Khripunoff et al., 2003).

3. Methods

This data set represents the first detailed direct measurements of turbidity currents in the deep ocean (Azpiroz-Zabala et al., 2017; Cooper et al., 2013). Ten flows were measured, with durations ranging from 8 h to over 9 days. Flow thicknesses varied from 16 m to 75 m, and flow velocities reached up to 2.3 m/s (Azpiroz-Zabala et al., 2017).

The data were collected using a 300 kHz acoustic Doppler current profiler (ADCP) anchored downstream of a meander bend in the Congo Canyon (Figure 1). The ADCP emits acoustic signals into the water column and computes averaged flow velocities over the acoustic footprint based on the Doppler shift (see supporting information). The ADCP was downward looking and moored 85 m above the seafloor from December 2009 to March 2010 (Figure 1). Velocities were measured every 5 s and vertically averaged over 2 m high grid cells called bins (Cooper et al., 2013).

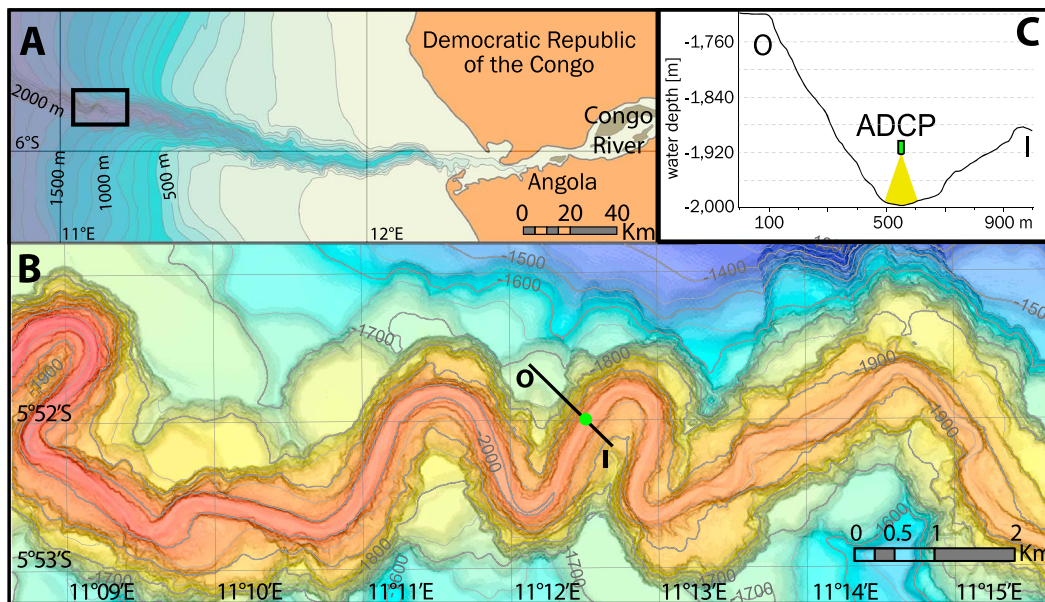


Figure 1. Location of the ADCP in the Congo Canyon. (a) Map of the Congo Canyon showing the study area (rectangle), with bathymetric contours in meters. (b) Detailed map showing the location of the instrumented mooring (green circle). Bold line indicates cross-canyon profile in Figure 1c. I and O denote the inner bend and outer bend, respectively. (c) Cross-canyon profile at deployment location showing acoustic Doppler current profiler (ADCP) suspended 85 m above the canyon floor.

We deduce the helical circulation from the vertical velocity profiles measured by the ADCP by calculating primary and secondary velocities. We define primary velocity as follows. First, we evaluate the flow direction for each ADCP velocity measurement binned by depth and average the velocities in this vertical profile to obtain the mean flow velocity direction. The primary velocity is then the component of velocity parallel to the mean velocity direction. We then define secondary velocity as the component of the velocity measurements perpendicular to the mean velocity direction (Rozovskii, 1957). In a similar way to previous studies of helical flows made with single moorings, we use the secondary velocity to infer the helical flow structure (Nidziko et al., 2009). The sign of the secondary velocity represents the direction of the secondary flow captured by the ADCP with positive values directed toward the outer bend and negative values toward the inner bend. The Rozovskii definition of secondary circulation assumes that the total outward directed velocity balances an equal total inward directed velocity. These secondary flow vectors define circulation cells that provide a two-dimensional view of the helical flow in the across-flow section (Figure 2).

The ADCP data were processed using the following steps (see supporting information for more detail):

1. Data were linearly interpolated from velocities of 0 m/s at the seabed to the velocity value of the lowest reliable measurement at 5 m above the seafloor (side lobe interference area, see supporting information).
2. The thickness of the flow is calculated following the integral relation by Ellison and Turner (1959).
3. The resultant vertical velocity profiles were depth averaged to obtain the average flow velocity and depth.
4. Primary and secondary velocities were calculated respectively as parallel and perpendicular to this average flow direction using the Rozovskii method (Rozovskii, 1957).
5. Results were averaged over 30 min to reduce sampling deviation of measurements.
6. Profiles influenced by tidal currents with magnitudes approaching that of the secondary circulation velocities were removed.
7. Patterns of helical flow were analyzed by arranging the data by flow thickness.

4. Results

We visualize and quantify helical flow in field-scale turbidity currents (Figure 2). The 10 measured flows vary in maximum thickness, duration, and primary velocity. Surprisingly, despite these variations, the secondary circulation pattern remains consistent among most flows (i.e., those 28–52 m thick; Figure 3). The secondary circulation comprises two vertically stacked cells, and this structure is independent of primary velocity and flow

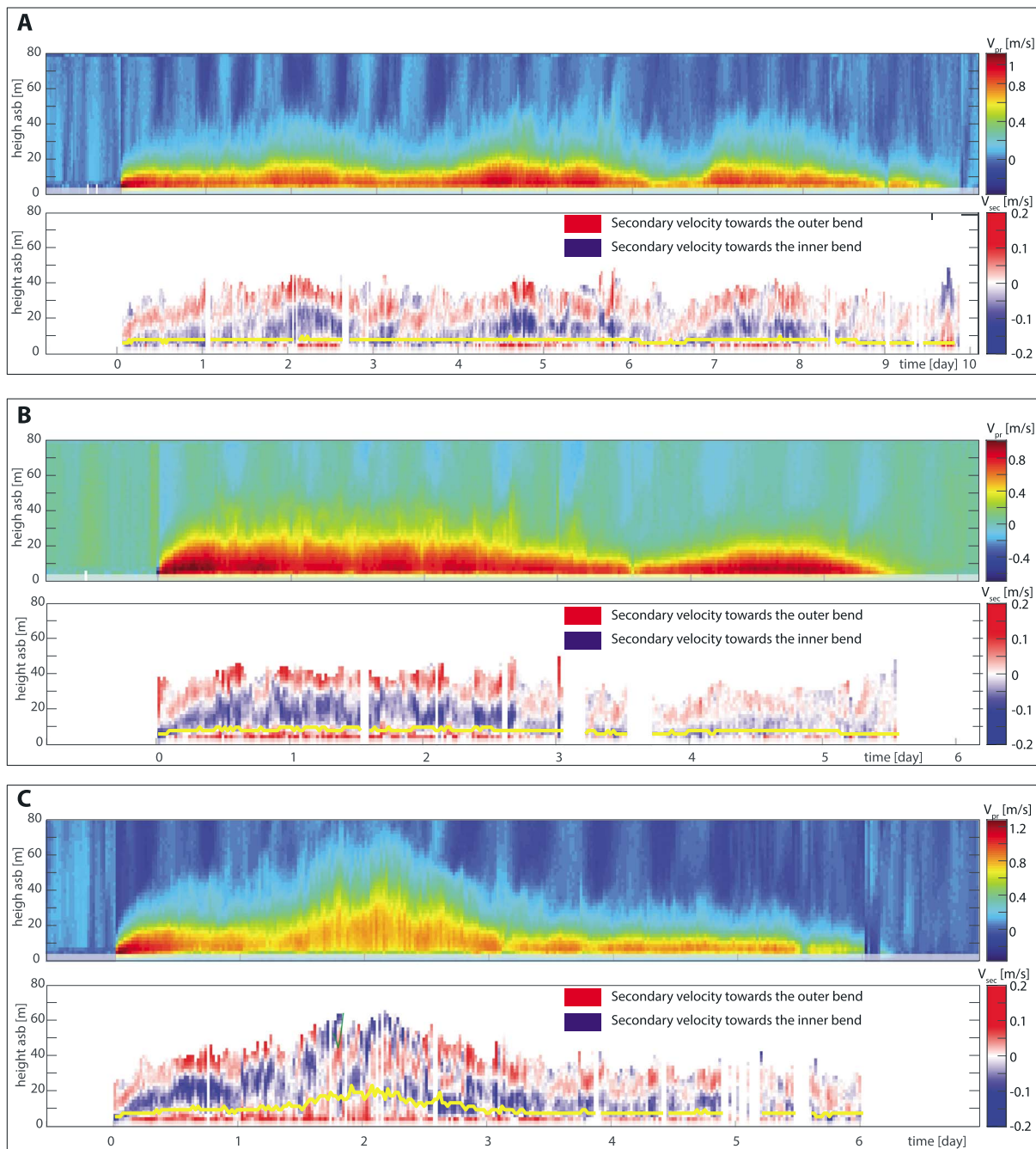


Figure 2. Primary (top) and secondary (bottom) velocities for three events recorded in the Congo Canyon. (a) Flow 1 is the longest duration flow. (b) Flow 4 shows the most stable secondary circulation structure. (c) Flow 10 is the fastest flow entirely recorded. Yellow lines in secondary velocity panels indicate height above the seabed (asb) of maximum velocity. Areas of side lobe interference are shaded at the bottom of each panel. Blank areas in secondary velocity panels define tidal currents (see supporting information).

thickness (Figure 3). The lower cell rotates in a river-reversed direction, counterclockwise when looking downstream, while the upper cell has the opposite rotation direction (Figure 2). In flows thinner than 28 m, the lower half of the bottom cell lies within the side lobe interference area and thus is not imaged accurately (see supporting information). Flows thicker than 52 m appear to lack a consistent two-cell pattern; this results from having few (<3) profiles with these thicknesses, and thus individual profiles having a disproportionate impact on the average pattern (Figure 3).

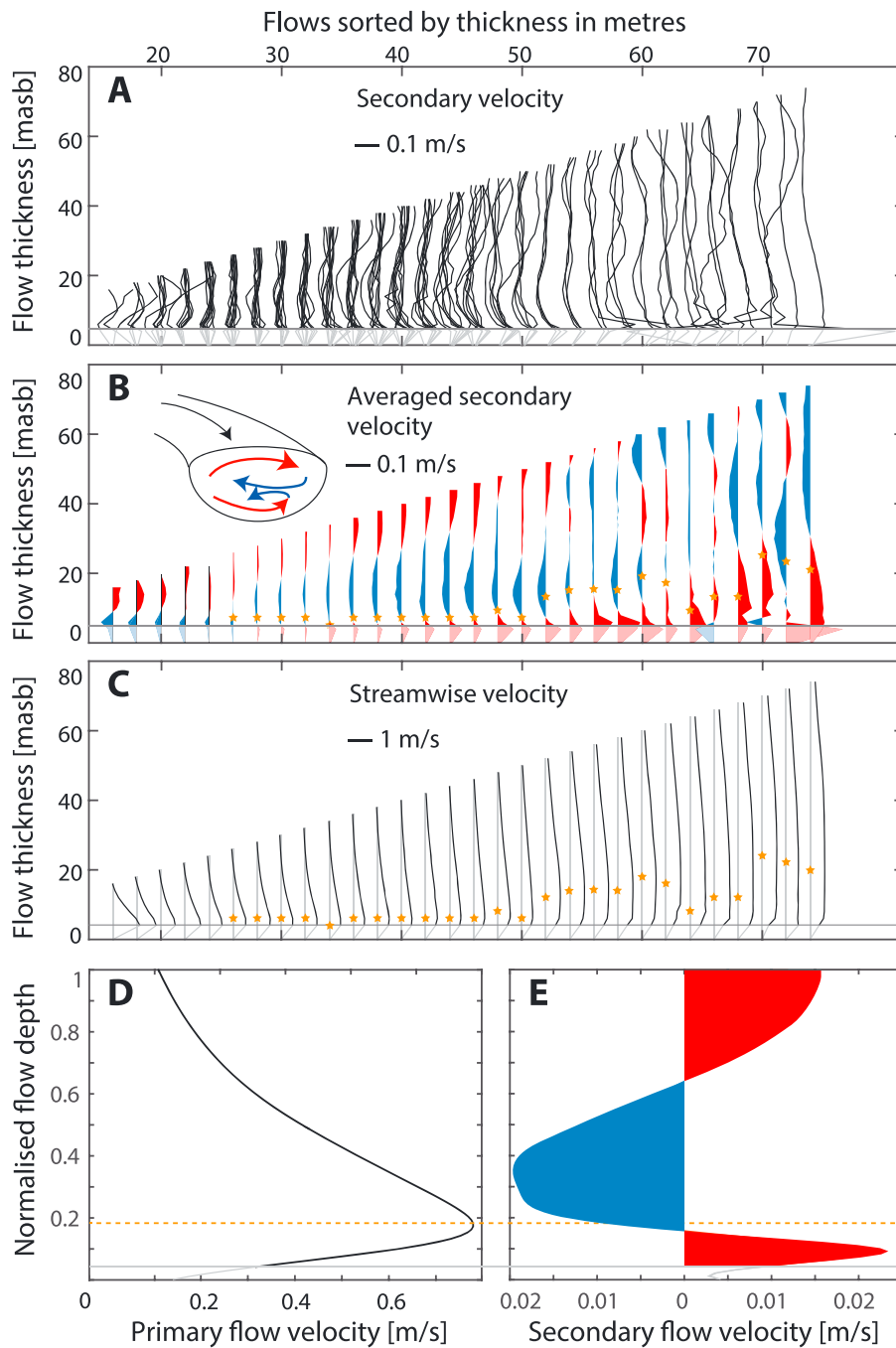


Figure 3. Profiles of the event-averaged primary and secondary velocity, which are ordered by flow thickness. (a) Event-averaged secondary velocity profiles arranged by their flow thickness. (b) Average of profiles shown in Figure 3a. Red colors denote positive secondary velocities, toward the outer bend. Blue colors denote negative secondary velocities, toward the inner bend. (c) Event-averaged primary velocity profiles arranged by their flow thickness. (d) Depth-normalized primary velocity profile, and (e) depth-normalized secondary velocity profile constructed by averaging over all available measurements. Normalization has been calculated according to flow depth and might bias averaged velocities toward faster velocities. Masb in x axis in Figures 3a–3c denotes meters above seabed. The yellow stars in Figures 3b and 3c indicate the height of the maximum primary velocity. Profiles in side lobe interference area are shown in gray. Horizontal gray line marks the top of side lobe interference area.

The average normalized secondary flow profile has maximum velocities from 0.02 to 0.09 m/s, which are 2–5% of the corresponding primary flow velocity. The same two-cell pattern holds for thinner flows (28–34 m thick); however, the magnitude of secondary circulation is lower. In all cases, the center of the low-ermost circulation cell corresponds to the height of the maximum primary velocity.

5. Discussion

5.1. Observations of Turbidity Currents Are Consistent With Previous Models of Stratified Saline Flows

Circulation cells form predominantly by the interaction of competing pressure gradients (Figures 4a–4c). In river-like circulation, centrifugal forces drive superelevation of the flow at the outer bend, generating a pressure gradient that drives near-bed flow toward the inner bend. River-like circulation can occur in density currents despite their near-bed velocity maximum because centrifugal acceleration moves the velocity maximum upward and outward (Sumner et al., 2014). In stratified saline density flows, an additional counter-acting pressure gradient is generated by dense fluid accumulating near the inner bend, which sets up a lateral pressure gradient that drives near-bed flow toward the outer bend (Figures 4a and 4b) (Nidzieko et al., 2009; Sumner et al., 2014; Umlauf & Arneborg, 2009). Such lateral pressure gradients may be enhanced by lateral velocity variations (Eggenhuisen & McCaffrey, 2012a). If the stratification-triggered pressure gradient dominates, then near-bed fluid is forced back toward the channel axis causing a river-reversed direction of rotation (Nidzieko et al., 2009; Sumner et al., 2014; Umlauf & Arneborg, 2009). It was hypothesized that this mechanism might apply to sediment-laden turbidity currents (Sumner et al., 2014)—we provide the first field data to support this.

5.2. Application of Saline Flow Model to Our Observations

Our measurements were collected downstream from a bend apex (Figure 1). Therefore, the measurements are the result of evolving processes operating within the bend. As the flow travels around the bend, it experiences a centrifugal force that causes flow superelevation at the outer bend, generating a pressure gradient toward the inner bend (Figure 4a). This generates a single, river-like cell that pushes suspended sediment toward the inner bend. Accumulation of sediment-laden fluid at the inner bend causes a lateral pressure gradient that opposes the flow of sediment-laden fluid toward the inner bend (Figure 4b). In our observations just downstream of the apex, the centrifugal acceleration decreases, and therefore the inwardly directed pressure gradient (caused by superelevation) decreases. Thus, the outwardly directed pressure gradient (caused by stratification) equals the original superelevation-driven force. Cross-stream near-bed flow must stop before switching to become outwardly directed as the centrifugal forces start to decrease (Figure 4c). Our suggested model contrasts with earlier models that proposed that switching of secondary flow direction occurred between bends (Giorgio Serchi et al., 2011; Peakall & Sumner, 2015). Also, rather than reversing the original direction of the flow cell, this process spawns a new river-reversed near-bed flow cell, which is located beneath the original river-like flow cell (Nidzieko et al., 2009). This produces the observed two-cell structure. The upper cell is driven by pressure gradients due to flow superelevation. The lower cell is driven by pressure gradients due to lateral stratification (Figures 2 and 3). The thickness of the bottom cell is controlled by the height that sediment is elevated when pushed toward the inner bend. We observe correlation between the heights of maximum downstream velocity and the center of the bottom cell. This probably results from difficulties in mixing sediment across the low turbulence zone around the velocity maximum in turbidity currents (Eggenhuisen & McCaffrey, 2012b).

5.3. A General Model for Helical Flow

In this section, we extend the above model to predict helical flow structure in a diverse array of geophysical flows, ranging from rivers to saline density flows and turbidity currents.

All flows experience centrifugally driven superelevation of their upper surface that creates a pressure gradient causing river-like helical flow (Figure 4a). This can cause accumulation of dense fluid or sediment toward the inner bend, which creates lateral stratification and causes an opposing pressure gradient back toward the outer bend (Figure 4b). We suggest that three potential scenarios exist (Figures 4d–4f), depending on which of these two pressure gradients dominate.

In scenario A (Figure 4d), a single weak river-like cell arises. The centrifugally driven pressure gradient displaces sediment to the inner bend as bed load but has insufficient energy to suspend the sediment. Therefore, there is no lateral stratification-driven pressure gradient back across the channel axis. We propose that scenario A occurs in bed load-dominated rivers and coarse-grained turbidity currents, and deposits point bars at the inner bend apex (Bagnold, 1977; Thorne et al., 1985).

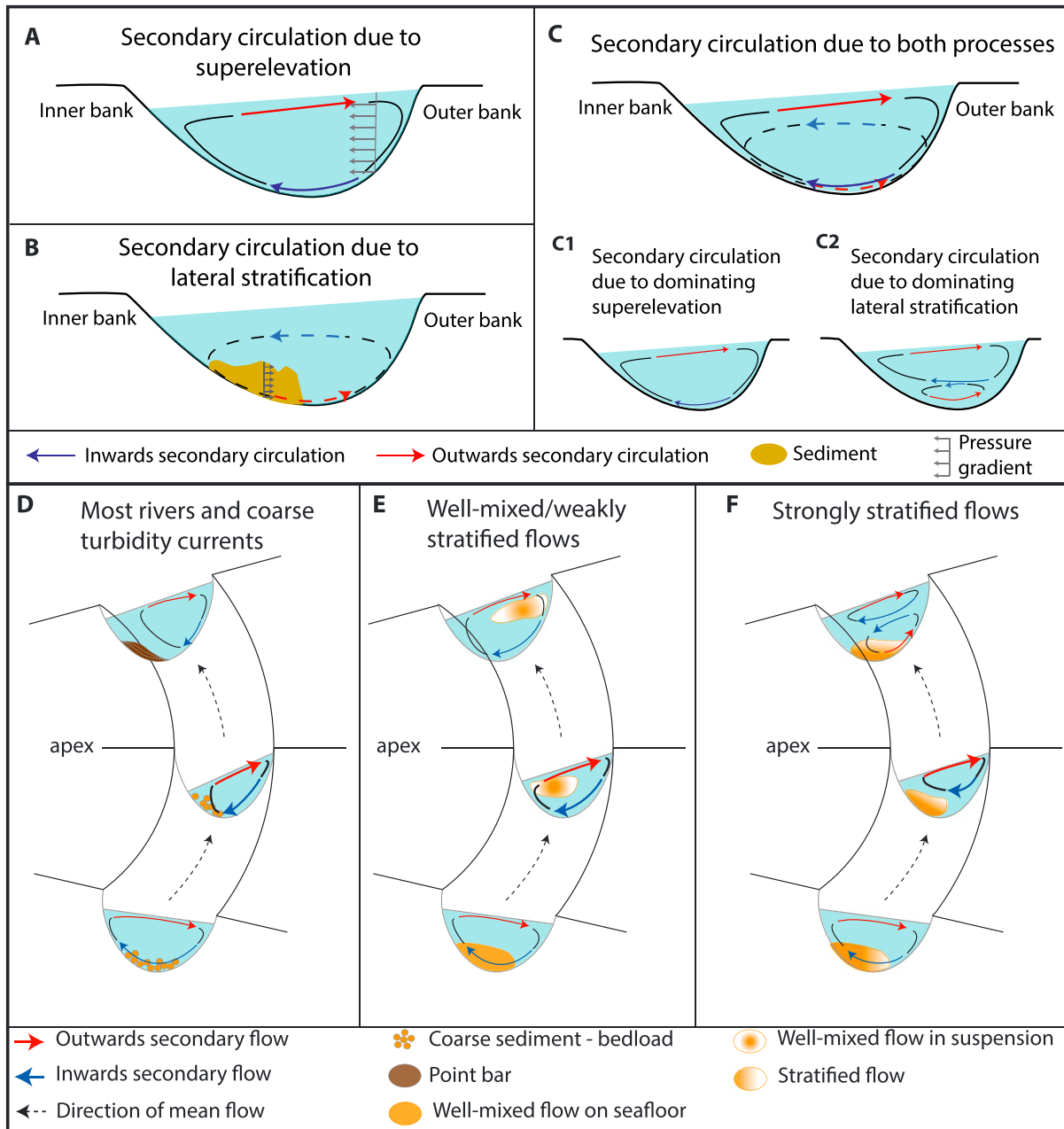


Figure 4. Schematic summary of secondary circulation patterns around a bend and their controls. Secondary circulation patterns result from competition between two main pressure gradients present in flows in bends. (a) Pressure gradient due to the water surface superelevation against the outer bend set up by centrifugal forces, and (b) pressure gradient due to stratification gradients in a density-stratified flow. Arrows denote resulting secondary flow patterns. Red denotes flow toward outer bend, and blue denotes flow toward inner bend, as in other figures. (c) Combination of secondary circulation cells due to superelevation and stratification pressure gradients in Figures 4a and 4b. Panel shows secondary circulation cells for two scenarios. The first scenario (c1) is when the pressure gradient due to superelevation is dominant, and the second scenario (c2) is when the pressure gradient due to density stratification is dominant. Schematic summaries of resultant secondary velocity around a bend. (d) Model for most rivers and coarse turbidity currents (scenario A), (e) model for well-mixed flows (scenario B), and (f) model for stratified flows (scenario C). Thickness of secondary circulation arrows denotes intensity of the flow.

In scenario B (Figure 4e), a single river-like cell is created. However, in this case the centrifugally driven pressure gradient is sufficient to move and suspend sediment at the inner bend. This results in a lateral stratification-driven pressure gradient that is smaller than the centrifugally driven pressure gradient. Thus, sediment remains in suspension and follows the streamlines of the circulation cell, causing overturning and mixing. We propose that scenario B occurs in well-mixed flows such as suspension-dominated rivers and saline flows, where sediment remains suspended with no deposition (Chikita, 1989; Nidziedo et al., 2009).

In scenario C (Figure 4f), two circulation cells are formed, with the lowermost cell showing river-reversed behavior. Here the centrifugally driven pressure gradient pushes sediment toward the inner bend. This stratification generates a lateral pressure gradient back across the channel. When the stratification-triggered pressure gradient is larger than the superelevation-triggered pressure gradient, cross-stream flow slows down and momentarily stops (Figures 4c and 4f). As the superelevation-generated pressure gradient decreases beyond the bend apex, the lateral pressure gradient due to sediment stratification causes suspended sediment to flow back toward the channel axis. This generates a new helical flow cell, beneath the original cell. This bottom cell is river-reversed and is initiated just downstream of the bend apex where centrifugal forces decline. Above the new lower cell, the original river-like cell continues to rotate (Figure 4f). We propose that scenario C occurs in strongly stratified rivers, saline flows and turbidity currents, and sediment deposits downstream of the bend apex (Chikita, 1989; Darby & Peakall, 2012; Nidziedo et al., 2009; Parsons et al., 2010; Wei et al., 2013).

5.4. Application of the General Model to a Range of Geophysical Flows

Our new model differs from previous models (Dorrell et al., 2013; Giorgio Serchi et al., 2011; Peakall & Sumner, 2015) with respect to (i) the location in the channel system where a second basal cell develops and (ii) the importance of confinement in secondary circulation. In addition, our new model predicts the helical flow structure across a diverse array of particle-laden or saline flow types.

Previous work suggested that the rotation direction of secondary circulation is constant around an individual bend and only changes its rotation direction between adjacent bends (Giorgio Serchi et al., 2011). Here we propose that this hypothesis holds for the upper helical flow cell, which is governed by centrifugal forces. However, when a lower helical flow cell develops, this reversed flow cell is generated just downstream of the bend apex. Second, we propose that the level of confinement of the channel systems plays an important role in secondary circulation. In confined systems, sufficiently stratified flows will show an upper river-like helical flow cell. However, in unconfined systems this upper cell may overspill and thus destroy itself, leading to a single river-reversed basal circulation cell (Dorrell et al., 2013).

This new general model can be applied to a large range of flows, from coarse-grained rivers to saline density flows. Here we discuss the implications of the model for understanding the architecture and the evolution of submarine channels. We consider the behavior of multiple turbidity currents with the same size and stratification traveling through an evolving submarine channel. We hypothesize that stratified turbidity currents will behave according to scenario C of our model. In this case, near-bed flow is driven toward the outer bend by pressure gradients generated by density stratification within the flow. Previous studies suggested (Peakall et al., 2000) that this type of secondary flow causes sediment to be deposited as point bars located downstream of bend apices. These point bars would increase the meander curvature, thus increasing the centrifugal forces and superelevation experienced by subsequent turbidity currents. However, once the pressure gradient toward the inner bend generated by superelevation exceeds the pressure gradient toward the outer bend generated by lateral stratification, then flow would switch to scenario B. In this case, near-bed flow is driven toward the inner bend by centrifugally driven pressure gradients. These pressure gradients exceed the lateral stratification-driven pressure gradients. As a consequence, the helical flow overturns sediment in suspension, thereby resulting in no deposition. At this point, the channel would cease meandering and its planform would become locked for flows of such size and stratification.

The largest submarine fans on Earth are fed by meandering channel systems. We propose that helical circulation around bends causes sediment to slosh from side to side or be overturned continuously, thereby helping to keep the sediment suspended over long distances. Together with fluid turbulence, helical flow thus plays a role in the extraordinary ability of turbidity currents to transport very large quantities of sediment for hundreds of kilometers.

References

- Abad, J. D., Sequeiros, O. E., Spinewise, B., Pirmez, C., Garcia, M. H., & Parker, G. (2011). Secondary current of saline underflow in a highly meandering channel: Experiments and theory. *Journal of Sedimentary Research*, 81(11), 787–813. <https://doi.org/10.2110/jsr.2011.61>
- Azpiroz-Zabala, M., Cartigny, M. J. B., Talling, P. J., Parsons, D. R., Sumner, E. J., Clare, M. A., ... Pope, E. (2017). Newly recognized turbidity current structure can explain prolonged flushing of submarine canyons. *Science Advances*, 3(10), e1700200. <https://doi.org/10.1126/sciadv.1700200>

Acknowledgments

We would like to thank Chevron for access to this exceptionally valuable data set. We thank Jon Wood (Ocean Data Technology) and others involved in building the mooring and collecting the data. M. A. was funded by National Oceanography Centre Southampton and Graduate School of National Oceanography Centre Southampton. M. J. B. C. and P. J. T. were supported by the Natural Environment Research Council projects NE/M017540/1, NE/K011480/1, NE/L009358/1, and NE/M007138/1. D. R. P. recognizes funding via HEIF at the University of Hull, and Natural Environment Research Council project NE/K011480/1. M. A. C. was funded by the Natural Environment Research Council grants NE/N012798/1 and NE/P009190/1. All data needed to evaluate the conclusions in the paper are presented in the paper and/or the supporting information. Additional data related to this paper may be requested from the authors.

- Bagnold, R. A. (1977). Bed load transport by natural rivers. *Water Resources Research*, 13(2), 303–312. <https://doi.org/10.1029/WR013i002p00303>
- Bolla Pittaluga, M., & Imran, J. (2014). A simple model for vertical profiles of velocity and suspended sediment concentration in straight and curved submarine channels. *Journal of Geophysical Research: Earth Surface*, 119, 483–503. <https://doi.org/10.1002/2013JF002812>
- Chikita, K. (1989). A field study on turbidity currents initiated from spring runoffs. *Water Resources Research*, 25(2), 257–271. <https://doi.org/10.1029/WR025i002p00257>
- Cooper, C., Wood, J., & Andrieux, O. (2013). Turbidity current measurements in the Congo Canyon. OTC 23992. Offshore technology conference, 6–9 may, Houston, Texas. 12 pp.
- Cooper, C., Wood, J., Imran, J., Islam, A., Wright, P., Faria, R., ... Casey, Z. (2016). Designing for turbidity currents in the Congo Canyon. OTC 26919, Offshore Technology Conference, 2–5 May.
- Corney, R. K. T., Peakall, J., Parsons, D. R., Elliot, L., Amos, K. J., Best, J. L., ... Ingham, D. B. (2006). The orientation of helical flow in curved channels. *Sedimentology*, 53(2), 249–257. <https://doi.org/10.1111/j.1365-3091.2006.00771.x>
- Corney, R. K. T., Peakall, J., Parsons, D. R., Elliot, L., Best, J. L., Thomas, R. E., ... Amos, K. J. (2008). Reply to discussion of Imran et al. on “The orientation of helical flow in curved channels” by Corney et al., *Sedimentology*, 55, 241–247.
- Cossu, R., & Wells, M. G. (2010). Coriolis forces influence the secondary circulation of gravity currents flowing in large-scale sinuous submarine channel systems. *Geophysical Research Letters*, 37, L17603. <https://doi.org/10.1029/2010GL044296>
- Darby, S. E., & Peakall, J. (2012). Modelling the equilibrium bed topography of submarine meanders that exhibit reversed secondary flows. *Geomorphology*, 163–164, 99–109. <https://doi.org/10.1016/j.geomorph.2011.04.050>
- Dorrell, R. M., Darby, S. E., Peakall, J., Sumner, E. J., Parsons, D. R., & Wynn, R. B. (2013). Superelevation and overspill control secondary flow dynamics in submarine channels. *Journal of Geophysical Research: Oceans*, 118, 3895–3915. <https://doi.org/10.1002/jgrc.20277>
- Eggenhuisen, J. T., & McCaffrey, W. D. (2012a). Dynamic deviation of fluid pressure from hydrostatic pressure in turbidity currents. *Geology*, 40(4), 295–298. <https://doi.org/10.1130/G32627.1>
- Eggenhuisen, J. T., & McCaffrey, W. D. (2012b). The vertical turbulence structure of experimental turbidity currents encountering basal obstructions: Implications for vertical suspended sediment distribution in non-equilibrium currents. *Sedimentology*, 59(3), 1101–1120. <https://doi.org/10.1111/j.1365-3091.2011.01297.x>
- Ellison, T. H., & Turner, J. S. (1959). Turbulent entrainment in stratified flows. *Journal of Fluid Mechanics*, 6(03), 423–448. <https://doi.org/10.1017/S0022112059000738>
- Ezz, H., & Imran, J. (2014). Curvature-induced secondary flow in submarine channels. *Environmental Fluid Mechanics*, 14(2), 343–370. <https://doi.org/10.1007/s10652-014-9345-4>
- Giorgio Serchi, F., Peakall, J., Ingham, D. B., & Burns, A. D. (2011). A unifying computational fluid dynamics investigation on the river-like to river-reversed secondary circulation in submarine channel bends. *Journal of Geophysical Research*, 116, C06012. <https://doi.org/10.1029/2010JC006361>
- Heezen, B. C., Menzies, R. J., Schneider, E. D., Ewing, W. M., & Granelli, N. C. L. (1964). Congo submarine canyon. *American Association of Petroleum Geologists Bulletin*, 48(7), 1126–1149.
- Huang, H., Imran, J., & Pirmez, C. (2012). The depositional characteristics of turbidity currents in submarine sinuous channels. *Marine Geology*, 329–331, 93–102.
- Imran, J., Islam, M. A., Huang, H., Kassem, A., Dickerson, J., Pirmez, C., & Parker, G. (2007). Helical flow couplets in submarine gravity underflows. *Geology*, 35(7), 659–662. <https://doi.org/10.1130/G23780A.1>
- Imran, J., Islam, M. A., & Kassem, A. (2008). “The orientation of helical flow in curved channels” by Corney et al., *Sedimentology*, Vol. 53, pp. 249–257 – Discussion. *Sedimentology*, 55, 235–239.
- Islam, M. A., & Imran, J. (2008). Experimental modeling of gravity underflow in a sinuous submerged channel. *Journal of Geophysical Research*, 113, C07041. <https://doi.org/10.1029/2007JC004292>
- Janocko, M., Cartigny, M. B. J., Nemeč, W., & Hansen, E. W. M. (2013). Turbidity current hydraulics and sediment deposition in erodible sinuous channels: Laboratory experiments and numerical simulations. *Marine and Petroleum Geology*, 41, 222–249. <https://doi.org/10.1016/j.marpetgeo.2012.08.012>
- Kassem, A., & Imran, J. (2004). Three-dimensional modeling of density current. II. Flow in sinuous confined and unconfined channels. *Journal of Hydraulic Research*, 42(6), 591–602. <https://doi.org/10.1080/00221686.2004.9628313>
- Keevil, G. M., Peakall, J., Best, J. L., & Amos, K. J. (2006). Flow structure in sinuous submarine channels: Velocity and turbulence structure of an experimental submarine channel. *Marine Geology*, 229(3–4), 241–257. <https://doi.org/10.1016/j.margeo.2006.03.010>
- Khripounoff, A., Vangriesheim, A., Babonneau, N., Crassous, P., Dennielou, B., & Savoye, B. (2003). Direct observation of intense turbidity current activity in the Zaire submarine valley at 4000 m water depth. *Marine Geology*, 194(3–4), 151–158. [https://doi.org/10.1016/S0025-3227\(02\)00677-1](https://doi.org/10.1016/S0025-3227(02)00677-1)
- Nidzicko, N. J., Hench, J. L., & Monismith, S. G. (2009). Lateral circulation in well-mixed and stratified estuarine flows with curvature. *Journal of Physical Oceanography*, 39(4), 831–851. <https://doi.org/10.1175/2008JPO4017.1>
- Normark, W. R. (1970). Growth patterns of deep-sea fans. *American Association of Petroleum Geologists Bulletin*, 54(11), 2170–2195.
- Parsons, D. R., Peakall, J., Aksu, A. E., Flood, R. D., Hiscott, R. N., Besiktepe, S., & Moulard, D. (2010). Gravity-driven flow in a submarine channel bend: Direct field evidence of helical flow reversal. *Geology*, 38(12), 1063–1066. <https://doi.org/10.1130/G31121.1>
- Peakall, J., McCaffrey, B., & Kneller, B. (2000). A process model for the evolution, morphology, and architecture of sinuous submarine channels. *Journal of Sedimentary Research*, 70(3), 434–448. <https://doi.org/10.1306/2DC4091C-0E47-11D7-8643000102C1865D>
- Peakall, J., & Sumner, E. J. (2015). Submarine channel flow processes and deposits: A process-product perspective. *Geomorphology*, 244, 95–120. <https://doi.org/10.1016/j.geomorph.2015.03.005>
- Pirmez, C., & Imran, J. (2003). Reconstruction of turbidity currents in Amazon Channel. *Marine and Petroleum Geology*, 20(6–8), 823–849. <https://doi.org/10.1016/j.marpetgeo.2003.03.005>
- Rozovskii, I. L. (1957). Flow of water in bends of open channels. Kiev, Academy of Sciences of the Ukrainian SSR, 233 pp.
- Savoye, B., Babonneau, N., Dennielou, B., & Bez, M. (2009). Geological overview of the Angola-Congo margin, the Congo deep-sea fan and its submarine valleys. *Deep-Sea Research Part II*, 56(23), 2169–2182. <https://doi.org/10.1016/j.dsr2.2009.04.001>
- Shepard, F. P. (1933). Submarine valleys. *American Geographical Society*, 23(1), 77–89.
- Straub, K. M., Mohrig, D., McElroy, B., & Buttles, J. (2008). Interactions between turbidity currents and topography in aggrading sinuous submarine channels: A laboratory study. *GSA Bulletin*, 120(3–4), 368–385. <https://doi.org/10.1130/B25983.1>
- Sumner, E. J., Peakall, J., Dorrell, R. M., Parsons, D. R., Darby, S. E., Wynn, R. B., ... White, D. (2014). Driven around the bend: Spatial evolution and controls on the orientation of helical bend flow in a natural submarine gravity current. *Journal of Geophysical Research: Oceans*, 119, 898–913. <https://doi.org/10.1002/2013JC009008>

- Talling, P. J., Allin, J., Armitage, D. A., Arnott, R. W. C., Cartigny, M. J. B., Clare, M. A., ... Xu, J. (2015). Key future directions for research on turbidity currents and their deposits. *Journal of Sedimentary Research*, *85*(2), 153–169. <https://doi.org/10.2110/jsr.2015.03>
- Talling, P. J., Wynn, R. B., Masson, D. G., Frenz, M., Cronin, B. T., Schiebel, R., ... Amy, L. A. (2007). Onset of submarine debris flow deposition far from original giant landslide. *Nature*, *450*(7169), 541–544. <https://doi.org/10.1038/nature06313>
- Thorne, C. R., Zevenbergen, L. W., Pitlick, J. C., Rais, S., Bradley, J. B., & Julien, P. Y. (1985). Direct measurement of secondary currents in a meandering sand-bed river. *Nature*, *316*, 746–747.
- Umlauf, L., & Arneborg, L. (2009). Dynamics of rotating shallow gravity currents passing through a channel. Part I: Observation of Transverse Structure. *Journal of Physical Oceanography*, *39*(10), 2385–2401. <https://doi.org/10.1175/2009JPO4159.1>
- Vangriesheim, A., Khripounoff, A., & Crassous, P. (2009). Turbidity events observed in situ along the Congo submarine channel. *Deep Sea Research, Part II*, *56*(23), 2208–2222. <https://doi.org/10.1016/j.dsr2.2009.04.004>
- Wei, T., Peakall, J., Parsons, D. R., Chen, Z., Zhao, B., & Best, J. (2013). Three-dimensional gravity-current flow within a subaqueous bend: Spatial evolution and force balance variations. *Sedimentology*, *60*(7), 1668–1680. <https://doi.org/10.1111/sed.12052>